# Thermal and structural analysis of Ni 50 Mn 50− x In x shape memory alloys

**Rim Ameur[1], Mahmoud Chemingui[1], Tarek Bachaga[1,3], Virgil Optasanu[2], Lluisa Escoda[3], Joan-Josep Suñol[3,*] and Mohamed Khitouni[1]**

[1]Laboratory of Inorganic Chemistry, UR 11-ES-73, University of Sfax, Fss, B.P. 1171, 3018 Sfax, Tunisia;

E-Mails: khitouni@yahoo.fr (M.K.); chmingui_mahmoud@yahoo.fr (M.C.); rimameur789@yahoo.fr (R. A.2

[2] ICB, UMR 6303 CNRS, Université de Bourgogne Franche Comté, 9 av. Alain Savary, 21078 Dijon Cedex,France

E-mail: Virgil.Optasanu@iut-dijon.u-bourgogne.fr

[3]Dep. de Física, Universitat de Girona, Campus de Montilivi, Girona 17017, Spain.

E-Mails: lluisa.escoda@udg.edu (L.E.), bachagatarak@yahoo.fr (T.B.)

*Correspondence: joanjosep.sunyol@udg.edu Tel.: +34-972-41-9757

Received: 02 February 2018; Accepted: date; Published: date

**Abstract:** Due to the high cost and low martensitic transformation temperature of Gallium as the basis for the most extensively studied Heusler alloys, the search for Ga-free alloys has been recently undertaken, particularly by introducing In, Sn or Sb. Therefore, three-shape memory alloys were obtained by rapid solidification: $Ni_{0.5}Mn_{0.5-x}In_x$ (x=0.12, 0.13 and 0.14). The thermal and structural analyses were performed by differential scanning calorimetry (DSC), X-ray diffraction (XRD) and electron microscopy scanning (SEM), which were applied to determine the martensite transformation. The structural transformations were found to be of austenitic-martensitic character, with the transformation temperatures decreasing with the increase of In content. The austenite state was proven to have a cubic $L2_1$ structure and the martensite was found to possess a monoclinic 10M structure. The obtained results have revealed that the control of the valence electron by atom (e/a) determines the functional properties displayed by these alloys near room-temperature and it is possible to develop alloys that can be candidates in a variety of applications such as sensors and actuators. Likewise, the entropy and enthalpy change linked to transformation are lower for $Ni_{50}Mn_{36}In_{14}$ alloy.

**Keywords:** Heusler alloys; Martensitic transformation; X-Ray diffraction; Rapid solidification; Thermodynamics.

## 1. Introduction

Heusler alloys are defined as ternary intermetallic compounds with $X_2YZ$ composition,[1] where X and Y are transition metals and Z is a III, IV, or V group element.[2] The ferromagnetic Heusler alloys $Ni_{50}Mn_{50-x}In_x$, with x within a certain range of concentration values have led to the observation of many interesting phenomena such as giant magnetocaloric effect (MCE),[3,4] large magnetoresistance (MR),[5,6] magnetic field-induced strain,[7] and exchange bias.[8,9] These alloys exhibit a first-order austenite–martensite phase transition, which is a cyclic process. By lowering the temperature, a cubic high-temperature parent austenite phase transforms into a tetragonal, orthorhombic or monoclinic structurally modulated martensite ordered by domains. By heating from the martensite state, the materials transform into austenite.[10]

Ni–Mn–Sn and Ni–Mn–In systems are of prospective importance as ferromagnetic-shape memory alloy. In the last decade, these alloys were produced as bulk polycrystalline ingots by arc melting followed by high-temperature homogenization annealing. Currently, ferromagnetic $Ni_{50}Mn_{50-y}X_y$ alloys with X = Sn and In can be directly produced as single-phase microcrystalline materials by rapid solidification using melt spinning technique.[11-13] The transition temperatures of shape-memory alloys strongly depend on the composition, and their values spread in a very wide range. In addition, it is well-known that the structures of martensite in Ni-Mn-In based alloys are sensitive to chemical composition. Temperature at which martensite starts and finishes its transformation into austenite, and vice versa, is usually referred to as $A_s$, $A_f$, and $M_s$, $M_f$, respectively. It has been reported that $M_s$ may decrease with a small increase in In content within the respective narrow intervals where both parent and product phases are magnetically ordered since it is quite dependent on the valence electron concentration e/a. For example, Sutou et *al.*[14] have found that $M_s$ decreases from 433 to 193

K when In content increases 0.10 to 0.15. Furthermore, Krenke et *al.*[15] have reported that the temperature Ms decreases from 760 to 264 K when the In content increases from 0.05 to 0.16.

In the present work, we consider three alloys in the Ni–Mn–In system (by modifying the chemical composition) to develop materials with a martensite–austenite transformation temperature range above, near, or below room temperature, with nominal composition $Ni_{50}Mn_{50-x}In_x$ (x= 0.12, 0.13 and 0.14). For these purposes, X-ray diffraction (XRD), differential scanning calorimetry (DSC) and Scanning electron microscopy (SEM), investigations were carried out on the ribbons produced by melt-spinning.

## 2. Experimental details

As-cast ingots of about 2 g with nominal composition $Ni_{0.5}Mn_{0.5-x}In_x$ (x=0.12, 0.13 and 0.14) were prepared by conventional argon arc melting from 99.98% pure Ni, 99.98% pure Mn, and 99.999% pure In, using Bühler MAM-1 compact arc melter. Each button ingot was melted five times and cast into a chilled copper mold to obtain a master rod with a diameter of 10 mm. The samples were induction-melted in quartz crucibles with a circular nozzle of 0.6 mm and then ejected onto a copper wheel rotating at a wheel linear speed of 48 $ms^{-1}$. The process was carried out in Argon environment. The obtained as-quenched ribbons were flakes of 1.2–2.0 mm in width and 4–12 mm in length. The prepared samples are named as follows: In0.12, In0.13 and In0.14, respectively.

The thermal and structural analyses were carried out by applying several techniques. In fact, X-ray diffraction (XRD) analyses were performed at room temperature with a Siemens D500 X-ray powder diffractometer using Cu-$K_\alpha$ radiation (Siemens, Berlin and Munich, Germany). The structure of samples was refined by using Maud Program[16] and software (Jana 2006, Jana, Praha, Czech Republic).[17] As for the thermal analyses, they were performed by differential scanning calorimetry (DSC) using a DSC830 calorimeter (Mettler Toledo, Greifensee, Switzerland) with a heating/cooling rate of 10 K/min working with a liquid nitrogen cooling system. Moreover, the microstructure and elemental chemical composition of ribbons were examined using a scanning electron microscope (SEM) via a DSM 960A microscope operating at 30 kV equipped with an X-ray energy dispersive spectroscopy (EDS) microanalysis system. To obtain a representative value of the average chemical composition for each alloy produced, a considerable number of ribbon flakes was characterized at room temperature.

## 3. Results and Discussion

### *3.1. SEM investigations*

The microstructural studies of $Ni_{0.5}Mn_{0.5-x}In_x$ (x=0.12, 0.13 and 0.14) ribbons were carried out employing scanning electron microscope. All samples present well-defined distinct layers of the cross-section. These sandwiched layers are those presenting the main differences in the microstructure of the three compositions (see Fig. 1). On the other hand, for In0.12 alloy micrographics, one can observe a columnar grains located at the ribbon free surface, which grew perpendicularly from small grains formed at the ribbon surface that was in contact with the wheel during the quenching process (see Fig. 1(a–c). This result has been previously observed in $Ni_{45.8}Mn_{42.6}In_{11.6}$ alloy ribbons.[18-19] The ribbon thickness has a size of ~15.58µm and the grain size of ~1.54µm. Figure 1 (d-f) shows the microstructure of the In0.13 sample that is also martensitic at room temperature. No phase separation can be identified, which is in good agreement with the x-ray diffraction patterns, where all reflections are related to the martensitic phases.

The measurements of grain thickness and size of In0.13 ribbon are around ~15.85µm and ~3.4µm, respectively. Moreover, the martensitic structure identified by XRD corresponds to a specific morphology in SEM analysis where the martensite is plate like (Fig. 1d). Although the martensite is plate-like, which can be recognized by the linear grain boundary of each plate, the thickness of the twins is different for In0.12 and In0.13. For In0.12 sample, a broad form was found, whereas for In0.13 sample, finer one was detected. In fact, within the grains, the plates order is parallel, as shown in Figs 1c and 1d. However, Fig 1i shows that for the case of In0.14 sample, the plates are not ordered between boards. Thereby, the measurements of grain thickness and size of In0.14 sample are around~16µm and ~3.72µm, respectively.

We can infer that ribbons are mostly composed of micronic columnar grains that grow through the whole ribbon thickness with the larger axis perpendicular to the ribbon plane. Therefore, ribbon microstructure is of columnar type with a high degree of orientation between adjacent grains. Samples are quite fragile and easy to cleave along the direction perpendicular to the ribbon plane. The comparison of their cross section columnar-like microstructure suggests that the presently produced Ni–Mn–In alloy exhibits faster grain growth kinetics as revealed by the larger in-plane grain width that roughly varies between 1 and 8µm.[13)]

Some EDS measurements were performed on each ribbon surface to check the homogeneity of the final composition. The EDS analyses of the As-spun ribbons are shown in Fig. 2(a,b,c). The results confirm the presence of mixed metallic elements. The composition analyses are found to accord well with the nominal compositions of the As-spun ribbons ((Ni0.498-Mn0.382-In0.120), (Ni0.505-Mn0.371-In0.130) and (Ni0.494-Mn0.365-In0.141)). Compositions are slightly shifted from the original. It is common in these alloys obtained by a two-step procedure: arc melting and melt spinning. A typical mapping analysis corresponding to In0.14 given in Fig. 2d demonstrates the homogeneity of the final composition.

### *3.2. XRD Investigations*

To determine the thermal analysis conditions, it is important to define crystal structure at room temperature. If the detected phase is cubic, the austenite–martensite transition must be found above room temperature, whereas if the detected phase is monoclinic, orthorhombic or tetragonal, the austenite– martensite transition must be found below by heating alloy. The structural parameters are determined by adjusting experimental patterns obtained by X-ray diffraction in temperature for all alloys and low temperature for the composition $Ni_{0.5}Mn_{0.36}In_{0.14}$ because it presents an austenitic structure at room temperature. For this reason, XRD patterns were collected at room temperature, see Figure 3. Alloys with In0.12 and In0.13 have a monoclinic 10M structure, whereas alloy with In0.14 has a cubic $L2_1$ structure. Miller indices were assigned with the aid of indexing programs as Treor and Dicvol. The crystal structures and the lattice constants obtained from X-ray diffraction experiments for samples are given in Table 1.

Figure 3 shows the diffraction patterns of the alloys with x=0.12 and 0.13. The reflections can be attributed to the 10M martensite structure. The inset shows the details in the range of 40°≤2θ≤46°, indicating that the unit cell is monoclinic with the I2/m space group. The corresponding crystallographic data related to the final convergence of the structural refinement are shown in Table 1. In order to know if the refinement has been done properly, it is not sufficient to check visually if experimental and theoretical diffractograms match. There are four reliability factors that give information about the accuracy of the refinement: $R_{structure\ factor}$, $R_{Bragg\ factor}$, $R_{pattern}$ (Rp) and $R_{weighted\ pattern}$ (Rwp).[20] The unit cell is monoclinic making an angle β=87.53°. 10M martensitic structure is characterized, in diffraction pattern, by the presence of four peaks around the principal reflection peak.

Alongside with the main reflections, additional peaks indicate the presence of structural modulation. Commonly, the ten-layer modulation (10M) is represented by a superstructure with ten adjacent unit cells along one of the crystallographic axes of the alloys with x=0.12

and x=0.13 (Fig.3). The parameter of dispersion with respect to the basic structure, austenitic of original type $L2_1$, in general, is an orthorhombic structure but for those alloys rich in Ni and/or Mn structure it is, generally, monoclinic 14M with symmetry space $P2_1/m$. In addition, the 14M structure is represented by a superstructure of seven adjacent cells along a crystallographic axis. Moreover, in the present work, the choice of alloys rich in nickel and manganese facilitates the obtention of a complex crystallographic structure at room temperature as martensitic monoclinic. As expected in Table 1, the lattice parameters of martensite increase slightly with the increase of Indium content.[10)] For x=0.14 the diffraction pattern shows a cubic $L2_1$ structure with a lattice parameter a = 0.5972 nm (see Table 1). Miller indices were assigned with the aid of indexing program as Treor and Dicvol. The presence of (111) and (311) superlattice diffraction peaks confirms the high order of $L2_1$ structure. The high/low degree of order might be ascribed to high/low vacancy concentration.[21)]

Therefore, these structural properties of both the austenite and the martensite are found to change with the increase in In content, obviously related to the smaller size of Mn atoms relative to that of In. In has an atomic radius of 0.167 nm, and Mn has an atomic radius of 0.140 nm. It appears that the considerably larger size of the In atom as compared to other group III-A and group IV-A elements leads to an Mn-Mn separation that is quite large.[15)] Besides, with the increase in In content: x=0.12, 0.13 and 0.14, excess Mn atoms occupy In sites. In such spatial configurations, Mn-Mn neighbors have a smaller separation than that in the stoichiometric compound.[15)] Therefore, we come to the conclusion that the variation of the crystal structure at room temperature from the structure 10M, to the austenitic cubic $L2_1$ structure depends on the In composition. In addition, modification of the production conditions and small changes in the composition can promote the thermal stability of different structures and, consequently, a different magnetoelastic behaviour. The small and constrained grains in the flakes might have made the transition to the martensite phase difficult and shifted it to lower temperatures, probably associated with the increased degree of quenched-in short-range disorder around defects, as proposed by Chernenko et *al*.[22] Obviously, factors as the slight shift in the valence electron concentrations also increase the structural complexity.

### *3.3. Thermal and thermodynamic analysis*

From XRD diffraction analysis, it is clear that DSC scans of alloys In0.12, In0.13 and In0.14 should be performed by heating from room temperature to detect the martensite–austenite transition. The martensitic transformation temperatures were determined by the intersection of the base line and the tangent line which is the largest slope of the peak, as illustrated in Figure 4. The obtained transformation temperatures are listed in Table 2. The hysteresis $\Delta T$ ($\Delta T = A_s - M_f$) is due to the increase in the elastic and the surface energy during the martensite formation. Thus, the nucleation of the martensite implies super-cooling. Therefore, it determined the width of the hysteresis, $\Delta T$, as the difference in the temperatures corresponding to the peak position, 3 K, 12K and 10K in alloys In0.12, In0.13 and In0.14, respectively. The transformation region can also be characterized by the martensite transformation temperature $T_0$: the temperature at which the Gibbs energies of the martensite and parent phases are equal [23]

$$T_0 = 1/2\,(M_s + A_f) \qquad (1)$$

This parameter of three samples is collected in Table 2.

The entropy ($\Delta S$) and enthalpy ($\Delta H$) changes in the structural transformations are calculated from calorimetry data[15] using the relationships:

$$\Delta H = \int_{T_i}^{T_f} \left(\frac{dQ}{dt}\right)\left(\frac{dT}{dt}\right)^{-1} dT \qquad (2)$$

and

$$\Delta S = \int_{T_i}^{T_f} \frac{1}{T}\left(\frac{dQ}{dt}\right)\left(\frac{dT}{dt}\right)^{-1} dT \tag{3}$$

where Ti and Tf are the temperature limits of integration.

The enthalpy and entropy changes values are also included in Table 2. It can be concluded that for both ΔS and ΔH, there is a significant concentration dependence. However, these thermodynamic parameters take their highest values for a concentration of In equal to 0.13. However, the In0.12 and In0.14 ribbons have the lowest values of ΔS and ΔH. Krenke et al.[15] have reported that in the case of Ni0.5Mn0.5-xInx alloy ingots, both ΔS and ΔH decrease with the increase of In concentration from x=0.05 to 0.25. They related this decrease to the large difference in the magnetic exchange interactions below and above Ms, which gave rise to a positive magnetic entropy change in the vicinity of martensitic transformation. The difference has been found between samples with different values of the injection over pressure or the distance between wheel and injection point.[22] On the other hand, one parameter used to characterize magnetic shape memory alloys is the electron-to-atom ratio (e/a) that is calculated using the electron concentration of the outer shells for each element of the Ni–Mn–In system. The number of electrons per atom for Ni, Mn and In atoms are 10 (3d8, 4s2), 7(3d5, 4s2) and 3(5s2, 5p1), respectively.

The following expression is used to calculate (e/a) ratio as described in detail in.[15]

$$(e/a)= [10x_{Ni}+ 7x_{Mn} +3x_{In}]/100 \tag{4}$$

where x is the atomic percentage of the element.

It is noted that the values decrease with the increase in the indium content (decreasing e/a), which is in agreement with the results obtained by other authors. The crystal structure of martensite formed in Ni-Mn-In alloys varies with alloy composition (or e/a). Besides, the change in the unit cell volume caused by the structural transformation would be different,[21] thus leading to the change of ΔS. In addition, it is known that there is a linear correlation between the average number of valence electrons per atom and the martensite start temperature Ms; it increases when the value (e/a) increases.[24-29] Similar behavior was found in this study, where the Ms temperature decreases from 431 to 260 K when e/a varies from 8.02 to 7.94 for In0.12 and In0.14, respectively. Hence, the control (e/a) determines the transformation temperatures range in this type of alloys. Furthermore, it is possible to develop alloys with the desired transformation temperatures as candidates for some applications such as sensors and actuators.

In addition to chemical composition, the atomic order of the parent phase has a great influence on the martensitic transformation. In this way, a relevant reduction in the transformation temperature extension, eventually associated with the local differences of atomic order, is obtained. For instance, Kreissl et al.[30] found that the disorder existing between Mn and Ga atoms in Ni2MnGa alloy substantially decreases Ms of about 100 K. On the other hand, what is original in our study in comparing the three sample curves, is that we can observe that the peaks of In0.12 and In0.13 alloy are more intense and exhibit a remarkable expansion and amplitude compared to that of In0.14 alloy. This result is similar to that reported in Ref.[15] in which the enthalpy and entropy change related to the transformation decreases as (e/a) decreases. The discrepancy with our study remains unclear but may be based on the influence of e/a ratio on the enthalpy and entropy change of martensitic transformation.[31] Further, it has been reported for Ni0.2+xMn0.1−xGa[32-33] that the character of the (e/a) dependence of $\Delta S$ is related to the magnetic contribution that relies on the difference in the magnetic exchange below and above Ms.

It is generally known that the magnetic exchange is closely connected to the Mn–Mn interatomic distance. However, it has been shown[34-36] that there is no significant concentration dependence for other systems such as MnNiSn, CuAlMn and Ni-Mn-Sn-Co Heusler alloys. On the other hand, Figure 4 reveals that with an increase in the indium content, the DSC scan was performed near room temperature and the cyclic process was close to room temperature. As expected, the austenite state for these alloys finish near room temperature because the martensite state starts at this temperature, allowing the resolution of the crystal structure of martensite product.[37)]

Likewise, from a thermodynamic point of view, there is an irreversible entropy, ΔSi, at the hysteretic transition. This irreversible entropy is proportional to the thermal hysteresis. It can be calculated by DSC data, taking into account the peak temperature of the austenite to martensite, TAM, and the martensite to austenite, TMA, temperatures. The formula as given in ref.[38)] is:

$$\frac{\Delta S_i}{\Delta S} = \frac{(T_{MA}-T_{AM})}{(T_{MA}+T_{AM})} \qquad (5)$$

As shown in Table 3, the values are lower than -0.02. Therefore, there is a small correction because usually differences obtained in ΔS by applying different ways are higher. A similar behavior was found in the literature in the Ni-Co-Mn-Sn system.[39)]

Furthermore, in the transformation energy there exists a term linked to the effect of the elastic contribution, ΔEel, which can be calculated by applying equation 6 in Ref.[40)]

$$\frac{\Delta E_{el}}{\Delta H} = \frac{(A_f-A_s)+(M_s-M_f)}{T_o} \qquad (6)$$

The values are small with the exception of sample with higher content of indium (Table 3). This alloy has also lower values of enthalpy and entropy. It is also known that the existence of different martensitic variants tends to minimize the elastic energy associated with the deformation of the sample. Thus, lower martensitic variants require greater energy expenditure to initiate the martensitic transformation.[41)] All these results are probably linked to a reduction of martensite variants in the samples.

## 4. Conclusions

In the present paper, we have investigated the martensitic transformation and the microstructure properties of the Ni0.5Mn0.5-xInx (x=0.12, 0.13 and 0.14) ribbons. Based on the obtained experimental results, some conclusions may be drawn.

The martensitic transformation temperature Ms increases as the e/a ratio decreases with the partial substitution of Ni by In.

The relationship (e/a) control permits the development of alloys with the desired transformation temperatures. Likewise, the entropy and enthalpy change related to the transformation decreases as (e/a) decreases.

Besides, SEM microstructures noted that the grain sizes increase with the increase in In content.

The microstructure shows the existence of equiaxial and columnar grains with a heterogeneous distribution, whereas the chemical composition is homogeneous.

The reduction in the average grain size is accompanied with a decrease in the start temperature of the martensitic transformation, Ms demonstrating that the structural transition temperatures can be tuned within certain limits by controlling this microstructural parameter. Furthermore, it is found that the transformation entropy is lower in the alloy produced at lower linear surface speed, probably due to the reduction of the relative temporal amount of material in contact with the wheel during the first stage of solidification. Minor entropy differences have been found between samples with different values of injection over pressure or the distance between wheel and injection point.

Acknowledgments: This study was financial supported by the MAT2013-47231-C2-2-P and Mat2016-75967- P projects. The authors would like to express their gratitude to Xavier Fontrodona Gubau for his XRD support. They would also like to thank Professor Leila

Mahfoudhi from the English Language Unit at the Faculty of Sciences of Sfax (Tunisia) for her constructive language polishing and editing services.

Author Contributions: R. Ameur is the PhD. Student, M. Khitouni and M. Chemingui are the supervisors of the thesis, J.J. Suñol contributed with DSC analysis, V. Optasanu and L. Escoda contributes with the SEM analysis supervision, T. Bachaga contributes with the XRD analysis discussion.

Conflicts of Interest: The authors declare no conflict of interest.

## References

1. Graf T., Casper F., Winterlik J., Balke B., Fecher, G.H. and Felser C. Anorg, Allg Chem. 635 (2009) 976-981.

2. Webster P.J. and Ziebeck K.R.A. in: H.R.J. Wijn (Ed.) Alloys and Compounds of d-Elements with Main Group Elements (Part 2. Landolt–Börnstein, New Series Group III). Springer Berlin. (1988) 19c, 75.

3. Aksoy S., Krenke T., Acet M., Wassermann E. F., Moya X., Manosa L. and Planes A. Appl. Phys. Lett. 91 (2007) 241916.

4. Sharma V.K., Chattopadhyay M.K., Shaeb K.H.B., Chouhan A. and Roy S.B. Appl Phys Lett. 89 (2006) 222509.

5. Kainuma R. Materials Transactions 59(03) (2018) 327-331.

6. Dubenko I., Ali N., Stadler S., Zhukov A., Zhukova V., Hernando B., Prida V., Prudnikov V., Ganshina E. and Granovsky A. Magnetic, Magnetocaloric, Magnetotransport, and Magneto-optical Properties of Ni–Mn–In-Based Heusler Alloys: Bulk, Ribbons, and Microwires, Chapter 2 in the hard-cover book: Novel Functional Magnetic Materials: Fundamentals and Applications (ed. A. Zhukov), Springer, Series in Materials Science. 231 (2016) 41-83.

7. Gao L., Shen X., Xu J.and Cai W. Materials Transactions 56(8) (2015) 1186-1191.

8. Krenke T., Duman E., Acet M., Wassermann E.F., Moya X. and Mañosa L. Phys Rev B. 75 (2007) 104414.

9. Dubenko I., Khan M., Arjun K.P., Bhoj R., Gautam S.S. and Naushad, A. J. Magn. Magn. Mat. 321 (2009) 754-757.

10. Bachaga T., Daly R., Escoda L. Suñol J.J. and Khitouni M. J Therm Anal Calorim. 122 (2015) 167–173.

11. Sànchez-Llamazares J.L., Sanchez T., Santos J.D., Perèz M.J., Sanchez M.L. and Hernando B. Appl Phys Lett. 92 (2008) 012513.

12. Santos J.D., Sànchez T., Alvarez P., Sànchez M.L., Sànchez-Llamazares J.L. and Hernando B. J Appl Phys. 103 (2008) 07B326.

13. Sànchez-Llamazares J.L., Hernando B., Garcıa C., Gonzalez J., Escoda L. and Suñol J.J. J. Phys D Appl Phys. 42 (2008) 045002.

14. Sutou Y., Imano Y., Koeda N., Omori T., Kainuma R., Ishida K. and Oikawa K. Appl Phys Lett. 85 (2004) 4358.

15. Krenke T., Acet M., Wassermann E.F., Moya X., Mañosa L. and Planes A. Phys Rev B. 73 (2006) 174413.

16. Lutterotti L. and Maud A. Rietveld analysis program designed for the internet and experiment integration. Acta Cryst. (2000) A56:s54.

17. Petrisek V. and Dusek M. Jana 2000: The crystallographic computing system. Institute of Physics: Prague, Czech Republic.

18. González L., García J., Nazmunnahar M., Rosa W.O., Escoda L., Suñol J.J., Prida V.M., Koledov V.V., Shavrov V.G. and Hernando B. Solid. Stat. Phen. 190 (2012) 307-310

19. González-Legarreta L., González-Alonso D., Rosa W.O., Caballero-Flores R., Suñol J.J, González J. and Hernando B. J. Magn. Magn. Mat. 383 (2015) 190–195.

20. Young R.A. The Rietveld method. Oxford University Press: International Union of Crystallography (1993).

21. Santamarta R, Cesari E, Font J, Muntasell J, Pons J, Dutkiewicz J. Scripta materialia. 54 (2006) 1985-1989.

22. Chernenko V.A., Cesari E., Pons J. and Seguı C. J Mater Res. 15 (2000) 1496–1504.

23. Kaufman L. and Hullert M. Thermodynamics of martensite transformation. In Olson GB, Owen WS Editors martensite Cambridge ASM International. (1992) 41–58.

24. Chernenko V.A. Scripta Mater. 40 (1999) 523–527.

25. Safaa N.S., Hamzah E., Abubakar T., Zamri M. and Tanemura M. J. Therm Anal Calorim. 118 (2014) 111–122.

26. Bachaga T., Daly R., Sunol J.J., Saurina J., Escoda L., Legarreta L.G., Hernando B. and Khitouni M. J. Supercond Nov Magn. 28 (2015) 3087–3092

27. Yildiz K., Kok M. J Therm Anal Calorim. 115 (2014) 1509–1514.

28. Kök M, Aydogdu Y. J Therm Anal Calorim. 113 (2013) 859–863.

29. Adorno A.T., Silva R.A.G. J Therm Anal Calorim. 83 (2006) 241–246.

30. Kreissl M, Neumann K.U., Stephens T. and Ziebeck K.R.A. J. Phys. Condens. Matter. 15 (2003) 3831–3839.

31. Wu Z., Liu Z., Yang H., Liu Y. and Wu G. Appl Phys. 44 (2011) 385403.

32. Khovailo V.V., Oikawa K., Abe T. and Tagaki T. J Appl Phys. 93 (2003) 8483–8485.

31. Wu S.K. and Yang S.T.. Mater. Lett. 57 (2003) 4291– 4296.

32. Coll R., Escoda L., Saurina J., Sànchez-Llamazares J.L., Hernando B. and Suñol J.J. J. Therm. Anal. Calorim. 99 (2010) 905–909.

33. Obrado E., Manosa L. and Planes A. Phys Rev B. 56 (1997) 20-23.

34. Deltell A., Escoda L., Saurina J. and Suñol J.J.. Metals. 5 (2015) 695-705.

35. Yan H., Zhang Y., Xu N., Senyshyn A., Brokmeier H.G., Esling C., Zhao X. and Zuo L. Act. Mater. 88 (2015) 375–388.

36. Wang G.F. Magnetic and Calorimetric Study of the Magenetocaloric Effect in Intermetallics Exhibiting First Order Magnetostructural Transitions. PhD. Thesis, University of Zaragoza, Zaragoza, Prensas Universitarias, Spain (2012).

37. Palacios E., Bartolomé J., Wang G., Burriel R., Skokov K. Taskaev S and Khovilo V. Entropy 17 (2015) 1236-1252.

38. Bachaga T., Daly R., Khitouni M., Escoda L., Saurina J. and Suñol J.J. Entropy 17 (2015) 646-657

39. Shamberger P.J. and Ohuchi F.S. Phys. Rev. B 79 (2009) 144407(1-9).

## Figures Captions

**Figure 1:** Typical SEM micrographs of the different regions: (a, d, i) Free surfaces, (b, e, j) Wheel surfaces and (c, f, k) Fractured cross sections of In0.12, In0.13 and In0.14 ribbons, respectively

**Figure 2:** EDS analyses of the as-spun ribbons (a) In0.12, (b) In0.13 and (c) In0.14 and (c) typical mapping analysis that corresponds to In0.14

**Figure 3:** X-ray diffraction patterns at room temperature for the alloys In0.12, In0.13 and In0.14.

**Figure 4:** DSC cyclic scans for the alloys In0.12, In0.13 and In0.14 at a heating/cooling rate of 10 K $min^{-1}$. Arrows indicate heating (down: austenite to martensite) and cooling (up: martensite to austenite).

## Tables captions

**Table 1:** Experimental details and refined crystallographic data for the samples with nominal composition $Ni_{0.5}Mn_{0.5-x}In_x$ (x=0.12, 0.13 and 0.14). The Reliability factors (profile residual, Rp, weighted profile residual Rwp and goodness of fit GOF=Rp/Rwp) for an excellent fit.

**Table 2:** Structural transition temperatures and the associated characteristic thermal parameters: (h) and (c) indicate calculated heating or cooling, respectively.

**Table 1**

| Sample | Symmetry | Space group | a/nm | b/nm | c/nm | Angle β/° | Rp /% | Rwp /% | GOF= Rp/Rwp |
|---|---|---|---|---|---|---|---|---|---|
| $Ni_{0.5}Mn_{0.38}In_{0.12}$ | Monoclinic 10M | I2/m | 0.431(4) | 0.568(5) | 2.100(1) | 87.53 | 11.94 | 10.86 | 1.09 |
| $Ni_{0.5}Mn_{0.37}In_{0.13}$ | Monoclinic 10M | I2/m | 0.434(3) | 0.572(4) | 2.124(2) | 87.58 | 11.14 | 10.84 | 1.02 |
| $Ni_{0.5}Mn_{0.36}In_{0.14}$ | Cubic $L2_1$ | Fm-3m | 0.597(2) | | | | 11.27 | 10.2 | 1.1 |

Table 2

| Sample | e/a | $M_s$/K | $M_f$/K | $A_s$/K | $A_f$/K | ΔT/K | $T_0$/K | ΔH/J $mol^{-1}$ | ΔS/J $mol^{-1}$ $K^{-1}$ |
|---|---|---|---|---|---|---|---|---|---|
| $Ni_{0.5}Mn_{0.38}In_{0.12}$ | 8.02 | 431 | 427 | 427 | 432 | 3 | 431.5 | 848.66±21(h)<br>410.25±12 (c) | 1.96±0.03 (h)<br>0.95±0.01 (c) |
| $Ni_{0.5}Mn_{0.37}In_{0.13}$ | 7.98 | 361 | 344 | 357 | 373 | 12 | 367 | 1038.13±41(h)<br>1031.02±11 (c) | 2.82±0.11 (h)<br>2.8±0.10 (c) |
| $Ni_{0.5}Mn_{0.36}In_{0.14}$ | 7.94 | 260 | 168 | 182 | 262 | 10 | 261 | 93.56±35 (h)<br>116.64±25 (c) | 0.35±0.01 (h)<br>0.44±0.01 (c) |

Figure 1

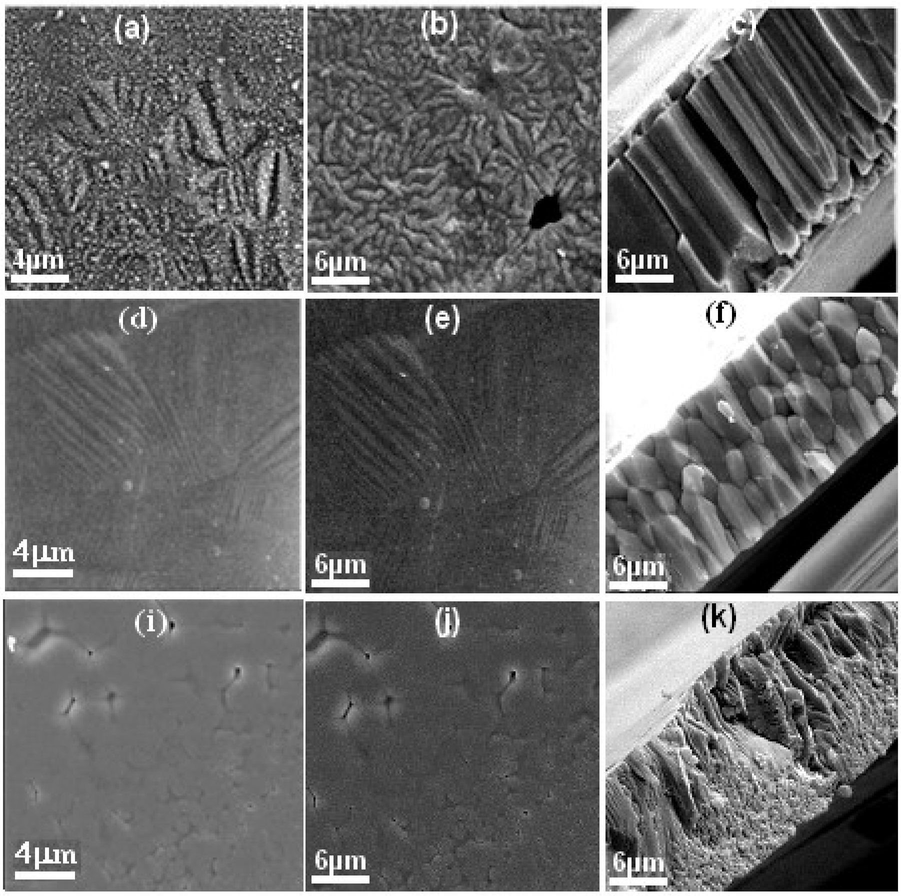

## Figure 2

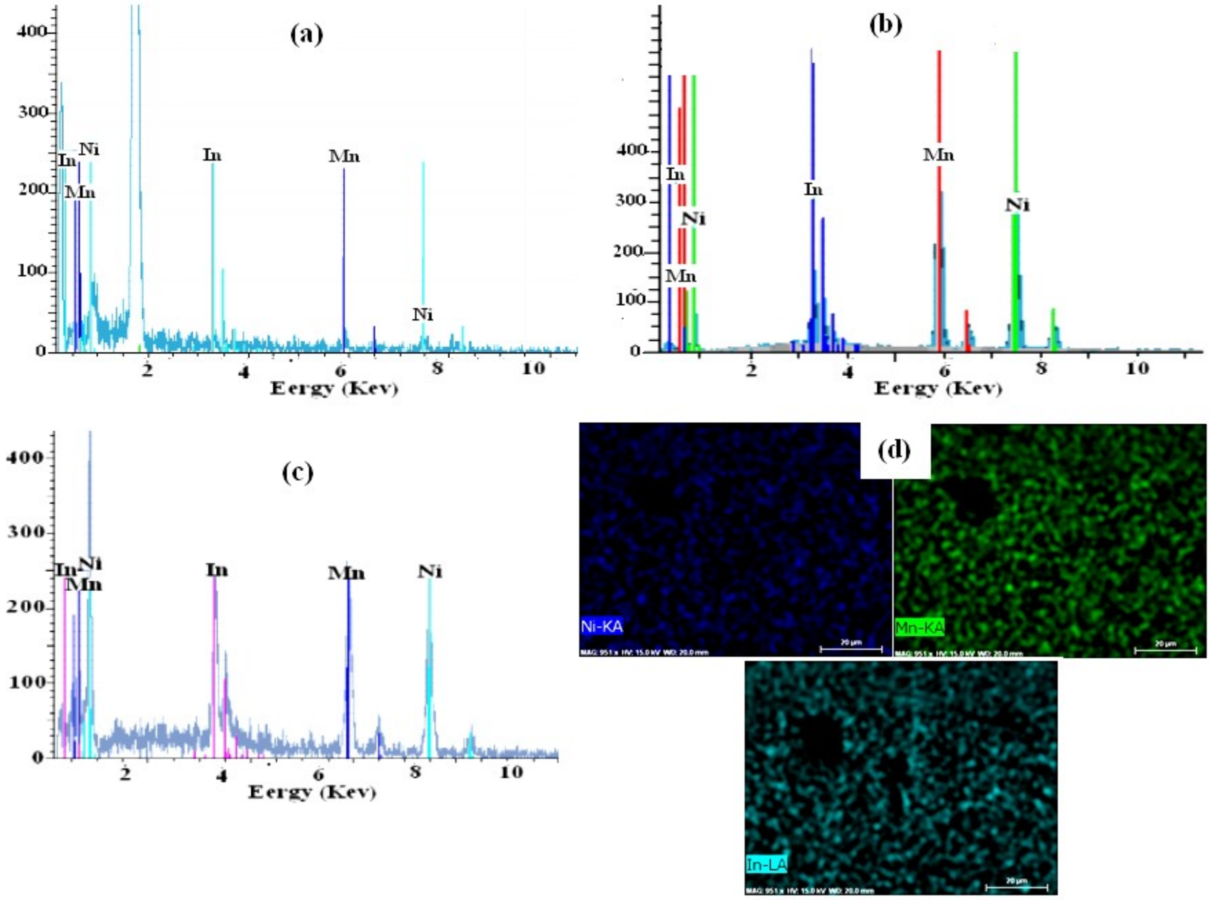

(a)
400
300
200
100
0
In
Ni
Mn
In
Mn
Ni
2
4
6
8
10
Eergy (Kev)
(b)
400
300
200
100
0
In
Ni
Mn
In
Mn
Ni
2
4
6
8
10
Eergy (Kev)
(c)
400
300
200
100
0
In
Ni
Mn
In
Mn
Ni
2
4
6
8
10
Eergy (Kev)
(d)
Ni-KA
Mn-KA
In-LA

Figure 3

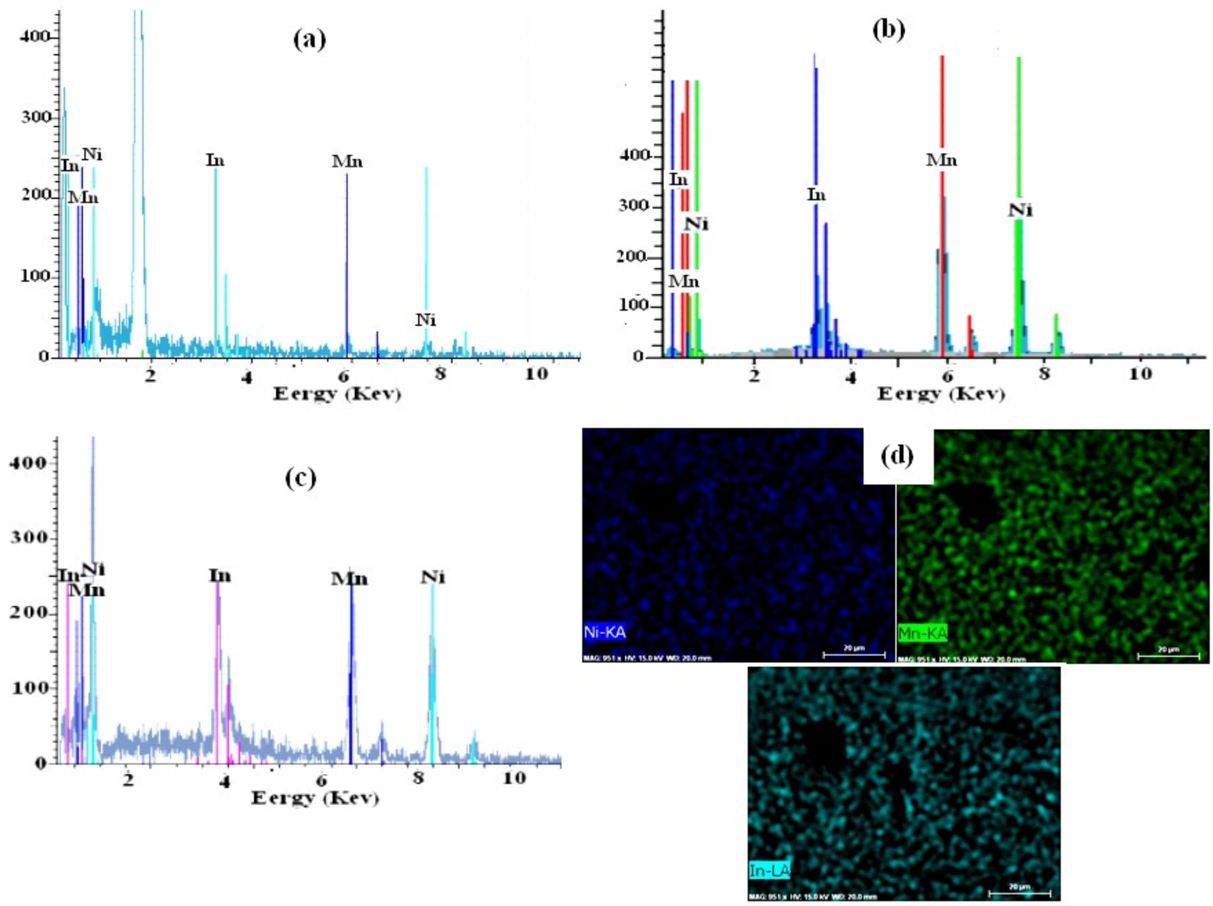

Figure 4

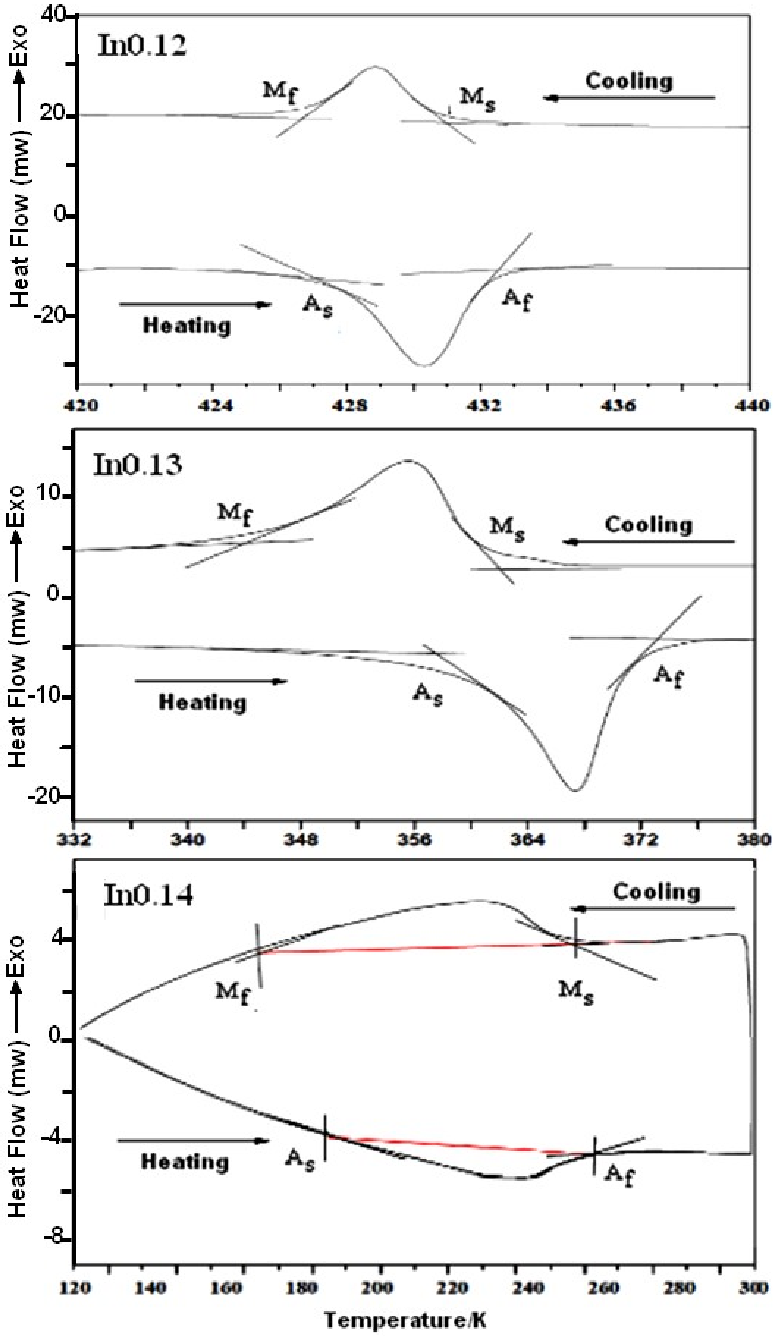
In0.12
Cooling
Heating
Mf
Ms
As
Af
Heat Flow (mw) ⟶ Exo
In0.13
Cooling
Heating
In0.14
Cooling
Heating
Temperature/K